


Discrete tomography in an in vivo small animal bone study

Elke Van de Castelele¹  · Egon Perilli² · Wim Van Aarle¹ · Karen J. Reynolds² · Jan Sijbers¹

Received: 18 October 2016 / Accepted: 10 January 2017 / Published online: 27 February 2017
© The Japanese Society for Bone and Mineral Research and Springer Japan 2017

Abstract This study aimed at assessing the feasibility of a discrete algebraic reconstruction technique (DART) to be used in in vivo small animal bone studies. The advantage of discrete tomography is the possibility to reduce the amount of X-ray projection images, which makes scans faster and implies also a significant reduction of radiation dose, without compromising the reconstruction results. Bone studies are ideal for being performed with discrete tomography, due to the relatively small number of attenuation coefficients contained in the image [namely three: background (air), soft tissue and bone]. In this paper, a validation is made by comparing trabecular bone morphometric parameters calculated from images obtained by using DART and the commonly used standard filtered back-projection (FBP). Female rats were divided into an ovariectomized (OVX) and a sham-operated group. In vivo micro-CT scanning of the tibia was done at baseline and at 2, 4, 8 and 12 weeks after surgery. The cross-section images were reconstructed using first the full set of projection images and afterwards reducing them in number to a quarter and one-sixth (248, 62, 42 projection images, respectively). For both reconstruction methods, similar changes in morphometric parameters were observed over time: bone loss for OVX and bone growth for sham-operated rats, although for

DART the actual values were systematically higher (bone volume fraction) or lower (structure model index) compared to FBP, depending on the morphometric parameter. The DART algorithm was, however, more robust when using fewer projection images, where the standard FBP reconstruction was more prone to noise, showing a significantly bigger deviation from the morphometric parameters obtained using all projection images. This study supports the use of DART as a potential alternative method to FBP in X-ray micro-CT animal studies, in particular, when the number of projections has to be drastically minimized, which directly reduces scanning time and dose.

Keywords Bone morphological parameters · Discrete tomography · X-ray micro-CT · Small animal imaging

Introduction

X-ray micro-computed tomography (micro-CT) enables non-destructive visualization of the internal structure of an object. By using projection images obtained from different angles around the object, virtual cross-sections (slices) are reconstructed through the sample, from which a 3D visualization can be created. In bone research, micro-CT is used to study pathologies, such as osteoporosis [1], osteoarthritis [2], rheumatoid arthritis [3], as well as bone tumors. It has also increasingly found its way in orthopedic research to assess biomaterials [4] and bone implants [5].

For in vivo small animal micro-CT imaging, it is important to minimize scanning time and the radiation dose given to the animal, in particular, if repeated scans are required. One way to achieve this is by reducing the number of projection images during scanning. For example, by acquiring only half or a quarter of the projection images, potentially

E. Van de Castelele and E. Perilli contributed equally to this work.

✉ Elke Van de Castelele
elke.vandecasteele@uantwerpen.be

¹ iMinds, VisionLab, Department of Physics, University of Antwerp (CDE), Universiteitsplein 1, Building N, 2610 Antwerp, Belgium

² Medical Device Research Institute, School of Computer Science, Engineering and Mathematics, Flinders University, GPO Box 2100, Adelaide, SA 5001, Australia

half or a quarter of the dose is given to the animal. However, this may introduce errors in the reconstructed cross-section image when utilizing traditional analytical algorithms such as that described by Feldkamp et al. [6], known as the filtered back-projection (FBP) method. Alternative reconstruction methods are the iterative algorithms [7], which consider the image reconstruction process as the optimization of a discrete representation of the object function in order to satisfy a system of equations that describes the imaging modality. They can provide reconstructions of higher quality compared to analytic methods, when only a limited number of projections are available [7]. Among these there is the discrete algebraic reconstruction technique (DART), which exploits a priori knowledge on the reconstructed grey levels. DART can provide high-quality reconstructions even with a small number of projections, as low as 10 [8]. Another advantage of discrete tomography is that the reconstruction directly computes the segmented (binarized) images necessary for the quantitative morphometric analysis, avoiding an additional segmentation step and selecting its threshold value. The DART algorithm has shown great potential in fields such as electron microscopy [9–11]. However, its application in X-ray micro-CT so far has been limited [12, 13]. In particular, it has never been explored in the field of in vivo micro-CT.

The aim of this manuscript is (1) to apply DART to repeated in vivo micro-CT scans performed on a rat model of osteoporosis, to explore DART's capability in detecting bone loss over time compared to the standard FBP technique; (2) to apply FBP and DART on the same scan data, however, by using progressively fewer projection images (1/4 and 1/6 of the original number of projections), and assess the respective capability of the two techniques in detecting bone loss.

Materials and Methods

Experimental setup

Animals

We used a subset of the micro-CT projection image datasets taken from a previously published study on female Sprague–Dawley rats by Perilli et al. [1]. Rats were 8 weeks of age at the beginning of the study (baseline). Two subgroups of rats were examined: a group with induced bone loss due to ovariectomy (OVX, $n = 3$) and a sham-operated group (SHAM, $n = 3$) that served as a control. The animals had been micro-CT scanned in vivo at five time points, i.e., at time of surgery (baseline) and at 2, 4, 8 and 12 weeks after surgery.

X-ray micro-CT acquisition

The projection image acquisition was performed in the previous study by using an in vivo X-ray micro-CT system (SkyScan 1076, SkyScan-Bruker, Kontich, Belgium), using a standard protocol for in vivo small animal studies [1]. Briefly, while under anesthesia, the right hind limb of each animal was placed into a cylindrical plastic holder to position the limb at the scanning midline and to prevent movement. The X-ray source voltage was set to 74 kVp/100 μ A and a 1-mm-thick aluminum filter was used for beam hardening reduction. An isotropic pixel size of 8.7 μ m was obtained for a 4000 \times 2096 CCD detector array, resulting in a total field of view of 35 \times 18 mm. The rotation step was 0.8° over 180°, leading to 248 projection images per scan (manufacturer default setting for in vivo scanning). The exposure time was 4.7 s and the total scan time per animal was 20 min at each time point [1].

Image reconstruction

All FBP and DART cross-section image reconstructions were performed first using the entire set of projection images, which was used as the ground truth, then 1/4 and then 1/6 of them (248, 62 and 42 projection images, respectively).

Image reconstruction using filtered back-projection (FBP)

For the standard FBP algorithm, the implementation of the SkyScan NRecon software was used to reconstruct a stack of 1200 cross-section images of 4000 \times 4000 pixels from each scan. The FBP algorithm reconstructs the cross-section images to a set of grey values, saved as 8-bit images (256 grey levels).

Pre-processing of the projection images was performed for beam hardening reduction, ring artifact correction, Gaussian smoothing and post-alignment (NRecon software, SkyScan). The NRecon software provides the option to export the projection images after pre-processing, so that these can be used by other reconstruction algorithms, in this case, DART. This way, both reconstructions (FBP and DART) used the same pre-processed projection images.

Image reconstruction using the discrete algebraic reconstruction technique (DART)

A 3D DART implementation was created in MATLAB based on the ASTRA Toolbox (University of Antwerp, Belgium), which provides the crucial projection operations, hardware accelerated with NVIDIA CUDA (NVIDIA Corporation, Santa Clara, CA, USA) [14–16].

The DART algorithm utilizes a priori knowledge of the grey levels (attenuation coefficients of the materials) present in the reconstructions, to achieve accurately segmented cross-section images. In the present study, from a radiological perspective, the scanning field of view contained mainly three types of materials: background (air), soft tissue and bone. Hence, the algorithm was set to reconstruct the cross-section images containing three grey values representing these three materials. These grey level values were first estimated from a standard FBP reconstruction of one rat at one time point at the end of the study, using the full projection dataset; these were then applied in all DART reconstructions. The estimation was done using a projection distance minimization method, which automatically finds the optimal threshold values of the (three) different materials in a sample using the projection images [17].

Morphological parameter calculations

The reconstructed datasets were then analyzed (software “CT-Analyser”, Version 1.13.2.1 64-bit, SkyScan–Bruker microCT). To perform trabecular morphometric analysis, typically two steps need to be applied on the reconstructed dataset: the selection of the trabecular volume of interest (VOI) and the binarisation of the grey-level images. For both FBP and DART datasets, the trabecular VOI was identical to the one used previously [1], containing only trabecular bone, starting at a distance of 1 mm from the lower end of the growth plate and extended distally for 350 cross-sections (3 mm in height). Binarisation was done on the FBP VOI datasets only (as the DART images are already thresholded), using global (uniform) thresholding [1]. A despeckle procedure was performed to remove isolated voxels (all objects smaller than 10 voxels, default value for CT-Analyser software). Over the binarised VOI datasets, the following histomorphometric parameters were calculated: bone volume fraction (BV/TV), trabecular thickness, separation and number (Tb.Th, Tb.Sp, Tb.N), and structure model index (SMI), a topological parameter. The number of objects (Obj.N) in 3D present in each VOI was also calculated (CT-Analyser).

Statistical analysis

The study sought: (1) For each reconstruction method, to compare each morphometric variable measured at a certain time point with the corresponding baseline, and to compare each variable measured at a given time point with the previous time point. For this, a Friedman test over the structural parameters was performed. If the p values for a given variable were found significant, a Mann–Whitney test was used to investigate time-related changes. (2) To assess the capability of each reconstruction method to distinguish the two

animal groups for a given number of projections; for this, the two groups were compared to each other at each time point (Mann–Whitney test). (3) To determine if within an animal group there were differences in the measured values that were due to the number of projections (all, 1/4, or 1/6 of the projections); a Friedman, followed by a Mann–Whitney test was performed at each time point. The alpha level for statistical significance was set at 0.05 for all the comparisons. Statistical analysis was performed using the Real Statistics Resource Pack software (Release 4.3; <http://www.real-statistics.com/>) for Microsoft Excel [18].

Results

Structural parameters describing the trabecular bone changes were calculated over the VOIs and compared for the different time points (Tables 1, 2). Figures 1 and 2 show transaxial cross-section images of a rat limb and the trabecular bone region of interest, respectively, in a SHAM rat reconstructed with the FBP and DART algorithms, at a decreasing number of projections. In Fig. 3, a 3D micro-CT rendering of the analyzed trabecular VOI of a rat from the SHAM and OVX group is shown at baseline and week 12, for the different reconstruction methods and numbers of projections.

In each animal group, the overall trend of the structural parameters over time was independent of the chosen reconstruction algorithm. For both reconstruction methods, in the OVX group, the BV/TV and Tb.N decreased significantly over time ($p < 0.05$), while the Tb.Sp and SMI increased (Fig. 4; Tables 1, 2). Instead, in the SHAM group, BV/TV, Tb.N and Tb.Th increased, whereas SMI decreased. Although the trend over time of the morphometric parameters in each group was independent of the reconstruction technique, the actual values differed between techniques. The BV/TV, Tb.Th and Tb.N obtained by DART were consistently higher than by FBP (for example, BV/TV was almost doubled in all DART reconstructions compared to FBP, Fig. 4).

Significant differences in morphometric parameters between the SHAM and OVX animals were detected from week 2 onwards, independent of the reconstruction method (Table 3). These differences between groups were, in general, preserved also with decreasing number of projections, for both reconstruction techniques. However, FBP reconstructions were more affected than DART, as follows (Table 4). For the FBP, when the number of projections was reduced, BV/TV was increased compared to the full projection dataset (in SHAM, the increase range was 6–23% or 19–53% when reduced to 1/4 or 1/6, respectively; in OVX, the increase was 10–23 or 30–58%), statistically significant at baseline (SHAM 1/6) and week 2 (OVX 1/6).

Table 1 Standard filtered back-projection (FBP): overview of the bone structural parameters calculated for each group over time. Comparisons are made between time points: the difference at each time point compared to its baseline and to the previous time point, respectively

	Baseline			Week 2			Week 4			Week 8			Week 12		
	Ave ± SD			Ave ± SD			Ave ± SD			Ave ± SD			Ave ± SD		
	All	¼	1/6	All	¼	1/6	All	¼	1/6	All	¼	1/6	All	¼	1/6
SHAM															
BV/TV (%)	7.73 ± 1.57	9.48 ± 1.78	11.83 ± 1.86	11.21 ± 1.77	12.51 ± 1.84	14.81 ± 2.02	13.70 ± 3.22	14.55 ± 3.21	16.33 ± 3.36	12.79 ± 5.09	13.88 ± 5.03	15.91 ± 4.80	20.44 ± 4.01	22.16 ± 3.16	24.54 ± 2.80
	(45*)	(32*)	(25)	(45*)	(32*)	(25)	(77*, 22)	(54*, 16)	(38, 10)	(65*, -7)	(46, -5)	(35, -3)	(164*, 60)	(134*, 60)	(108*, 54*)
Tb.Th (µm)	52 ± 1	50 ± 1	50 ± 1	65 ± 3	59 ± 2	57 ± 2	77 ± 8	67 ± 6	64 ± 5	77 ± 10	65 ± 8	62 ± 7	82 ± 11	70 ± 8	66 ± 5
	(26*)	(18*)	(15*)	(26*)	(18*)	(15*)	(48*, 18*)	(35*, 15*)	(28*, 11*)	(49*, 1)	(31*, -3)	(24*, -3)	(59*, 7)	(39*, 7)	(32*, 7)
Tb.Sp (µm)	297 ± 45	241 ± 35	188 ± 21	274 ± 29	223 ± 21	176 ± 12	289 ± 37	239 ± 33	186 ± 20	310 ± 51	232 ± 24	183 ± 15	231 ± 18	176 ± 16	143 ± 12
	(-7)	(-7)	(-6)	(-7)	(-7)	(-6)	(-3, 5)	(-1, 7)	(-1, 6)	(5, 7)	(-4, -3)	(-3, -2)	(-22*, -25*)	(-27*, -24*)	(-24*, -22*)
Tb.N (mm ⁻¹)	1.49 ± 0.29	1.89 ± 0.33	2.36 ± 0.34	1.72 ± 0.23	2.12 ± 0.26	2.57 ± 0.29	1.78 ± 0.28	2.15 ± 0.33	2.54 ± 0.37	1.62 ± 0.43	2.09 ± 0.50	2.53 ± 0.48	2.48 ± 0.34	3.20 ± 0.41	3.71 ± 0.43
	(15)	(12)	(9)	(15)	(12)	(9)	(19, 3)	(13, 1)	(8, -1)	(9, -9)	(10, -2)	(7, 0)	(67, 53)	(69, 53)	(57, 47)
SMI	2.4 ± 0.1	2.5 ± 0.1	2.6 ± 0.1	2.3 ± 0.1	2.4 ± 0.1	2.5 ± 0.1	2.2 ± 0.1	2.3 ± 0.1	2.5 ± 0.1	2.3 ± 0.2	2.5 ± 0.3	2.6 ± 0.2	2.0 ± 0.3	2.1 ± 0.3	2.1 ± 0.2
	(-4)	(-3)	(-2)	(-4)	(-3)	(-2)	(-7, -4)	(-7, -4)	(-3, -1)	(-2, 6)	(-1, 7)	(0, 3)	(-16, -15)	(-16, -16)	(-18, -18)
OVX															
BV/TV (%)	8.97 ± 3.88	10.67 ± 3.74	13.08 ± 3.81	6.15 ± 0.78	7.57 ± 0.70	9.70 ± 0.87	3.50 ± 1.49	4.21 ± 1.76	5.32 ± 2.14	3.50 ± 2.79	3.86 ± 2.95	4.54 ± 3.18	3.00 ± 1.92	3.36 ± 2.23	4.10 ± 2.69
	(-32)	(-29)	(-26)	(-32)	(-29)	(-26)	(-61, -43)	(-61*, -44*)	(-59*, -45*)	(-61, 0)	(-64, -8)	(-65*, -15)	(-67, -14)	(-69*, -13)	(-69*, -10)
Tb.Th (µm)	57 ± 6	53 ± 5	52 ± 5	58 ± 2	53 ± 2	52 ± 2	60 ± 4	54 ± 3	51 ± 4	71 ± 6	62 ± 5	57 ± 6	78 ± 7	66 ± 6	59 ± 4
	(2)	(0)	(-1)	(2)	(0)	(-1)	(5, 2)	(2, 2)	(-3, -2)	(25, 20)	(18, 16)	(9, 12)	(38, 10)	(25, 6)	(13, 4)
Tb.Sp (µm)	308 ± 77	241 ± 49	186 ± 25	374 ± 45	282 ± 32	210 ± 17	800 ± 295	521 ± 149	301 ± 41	1023 ± 376	735 ± 300	363 ± 69	1078 ± 330	685 ± 221	348 ± 70
	(21)	(17)	(13)	(21)	(17)	(13)	(160*, 114*)	(116*, 85*)	(62*, 43*)	(232*, 28)	(205*, 41)	(95*, 21)	(250*, 5)	(184*, -7)	(87*, -4)
Tb.N (mm ⁻¹)	1.54 ± 0.51	1.99 ± 0.52	2.46 ± 0.50	1.05 ± 0.10	1.43 ± 0.11	1.87 ± 0.15	0.58 ± 0.22	0.77 ± 0.30	1.03 ± 0.37	0.48 ± 0.34	0.60 ± 0.41	0.77 ± 0.46	0.39 ± 0.27	0.52 ± 0.37	0.70 ± 0.46
	(-32)	(-28)	(-24*)	(-32)	(-28)	(-24*)	(-62*, -45*)	(-61*, -46*)	(-58*, -45*)	(-69*, -18)	(-70*, -22)	(-69*, -26)	(-74*, -17)	(-74*, -14)	(-72*, -9)
SMI	2.4 ± 0.2	2.5 ± 0.2	2.5 ± 0.2	2.6 ± 0.1	2.7 ± 0.1	2.7 ± 0.0	2.6 ± 0.1	2.8 ± 0.1	3.0 ± 0.1	2.6 ± 0.2	2.8 ± 0.2	3.2 ± 0.3	2.6 ± 0.1	2.9 ± 0.1	3.4 ± 0.3
	(7)	(7)	(9*)	(7)	(7)	(9*)	(10, 3)	(12*, 4)	(19*, 9*)	(9, -1)	(11, 0)	(25*, 6)	(8, -1)	(14*, 3)	(35*, 8)

In parentheses, week 2: (percent difference to baseline); in parentheses, weeks 4, 8, 12: (percent difference to baseline, percent difference to the previous time point)

Ave average, SD standard deviation

* *p* < 0.05, Mann–Whitney test

Table 2 Discrete tomography (DART): Overview of the bone structural parameters calculated over time for each group. Comparisons are made between the time points: the difference at each time point compared to its baseline and to the previous time point, respectively

	Baseline			Week 2			Week 4			Week 8			Week 12		
	Ave	± SD	All	1/6	1/4	1/6	Ave	± SD	All	1/6	1/4	1/6	Ave	± SD	All
SHAM															
BV/TV (%)	21.85 ± 2.63	22.92 ± 2.76	23.31 ± 2.60	25.21 ± 2.11	26.20 ± 2.15	26.79 ± 2.18	26.14 ± 3.96	26.99 ± 4.20	27.47 ± 3.95	27.51 ± 4.26	28.30 ± 4.53	29.23 ± 4.48	35.51 ± 3.17	36.54 ± 3.22	37.35 ± 3.31
				(15)	(14)	(15)	(20, 4)	(18, 3)	(18, 3)	(26*, 5)	(23, 5)	(25*, 6)	(62*, 29)	(59*, 29)	(60*, 28)
Tb.Th (µm)	74 ± 1	85 ± 2	92 ± 2	84 ± 4	92 ± 4	99 ± 4	95 ± 5	100 ± 5	106 ± 5	93 ± 8	101 ± 7	109 ± 8	103 ± 7	110 ± 5	116 ± 2
				(13*)	(9*)	(7*)	(28*, 13*)	(18*, 9)	(15*, 7)	(25*, -2)	(19*, 1)	(18*, 3)	(38*, 10)	(29*, 8)	(26*, 6)
Tb.Sp (µm)	207 ± 31	203 ± 24	202 ± 20	192 ± 12	188 ± 11	191 ± 14	219 ± 34	210 ± 25	219 ± 27	196 ± 14	212 ± 19	230 ± 22	177 ± 24	172 ± 19	181 ± 15
				(-7)	(-7)	(-6)	(6, 14)	(3, 12)	(8, 15)	(-5, -10)	(4, 1)	(14, 5)	(-14, -9)	(-15, -19*)	(-11, -21*)
Tb.N (mm ⁻¹)	2.93 ± 0.32	2.69 ± 0.28	2.52 ± 0.24	2.99 ± 0.15	2.84 ± 0.16	2.72 ± 0.16	2.75 ± 0.38	2.68 ± 0.34	2.59 ± 0.30	2.94 ± 0.25	2.78 ± 0.26	2.67 ± 0.23	3.47 ± 0.38	3.34 ± 0.31	3.21 ± 0.23
				(2)	(5)	(8)	(-6, -8)	(0, -5)	(3, -5)	(0, 7)	(3, 4)	(6, 3)	(18, 18)	(24*, 20)	(27*, 20*)
SMI	1.9 ± 0.1	2.2 ± 0.1	2.3 ± 0.1	1.9 ± 0.1	2.1 ± 0.1	2.2 ± 0.1	1.8 ± 0.1	2.0 ± 0.2	2.0 ± 0.2	1.9 ± 0.2	1.9 ± 0.2	1.9 ± 0.2	1.3 ± 0.1	1.5 ± 0.2	1.5 ± 0.2
				(-1)	(-4)	(-7)	(-7, -6)	(-8, -5)	(-12*, -5)	(-1, 7)	(-12*, -4)	(-16*, -5)	(-30, -30)	(-31*, -21)	(-35*, -22)
OVX															
BV/TV (%)	23.27 ± 4.63	24.52 ± 4.61	25.06 ± 4.73	19.25 ± 1.57	19.92 ± 1.59	20.55 ± 1.39	11.14 ± 4.08	11.18 ± 4.29	11.57 ± 4.31	8.80 ± 6.56	8.53 ± 6.73	8.79 ± 6.71	8.10 ± 6.41	8.23 ± 6.67	8.53 ± 7.01
				(-17)	(-19)	(-18)	(-52*, -42*)	(-54*, -44*)	(-54*, -44*)	(-62*, -21)	(-65*, -24)	(-65*, -24)	(-65*, -8)	(-66*, -3)	(-66*, -3)
Tb.Th (µm)	78 ± 5	89 ± 3	97 ± 3	78 ± 1	88 ± 1	95 ± 1	78 ± 3	89 ± 2	96 ± 3	86 ± 4	98 ± 2	103 ± 4	97 ± 4	104 ± 4	109 ± 2
				(1)	(-2)	(-2)	(0, -1)	(0, 2)	(-1, 1)	(11, 11)	(10*, 10*)	(6, 7*)	(24, 12)	(17*, 6*)	(13*, 6*)
Tb.Sp (µm)	206 ± 42	209 ± 44	211 ± 40	243 ± 47	239 ± 36	239 ± 34	670 ± 380	711 ± 389	609 ± 289	950 ± 462	948 ± 407	993 ± 392	1043 ± 398	1014 ± 419	1011 ± 375
				(18)	(15)	(13)	(226*, 176*)	(241*, 197*)	(188*, 155*)	(362*, 42)	(354*, 33)	(370*, 63)	(407*, 10)	(386*, 7)	(378*, 2)
Tb.N (mm ⁻¹)	2.98 ± 0.40	2.74 ± 0.41	2.58 ± 0.40	2.45 ± 0.20	2.27 ± 0.19	2.17 ± 0.17	1.43 ± 0.50	1.25 ± 0.47	1.20 ± 0.46	1.00 ± 0.69	0.86 ± 0.66	0.85 ± 0.63	0.86 ± 0.71	0.80 ± 0.67	0.78 ± 0.63
				(-18)	(-17)	(-16)	(-52*, -42*)	(-55*, -45*)	(-53*, -44*)	(-67*, -30)	(-69*, -31)	(-67*, -29)	(-71*, -14)	(-71*, -7)	(-70*, -8)
SMI	1.9 ± 0.2	2.1 ± 0.2	2.2 ± 0.2	2.1 ± 0.0	2.3 ± 0.1	2.4 ± 0.1	2.2 ± 0.1	2.4 ± 0.1	2.6 ± 0.0	2.1 ± 0.1	2.4 ± 0.3	2.5 ± 0.4	2.3 ± 0.2	2.5 ± 0.3	2.6 ± 0.4
				(11*)	(11)	(10)	(15*, 4)	(16, 5)	(16, 5)	(15*, 0)	(16, 0)	(14, -2)	(25*, 9)	(19, 2)	(18, 4)

In parentheses, week 2: (percent difference to baseline), in parentheses, weeks 4, 8, 12: (percent difference to baseline, percent difference to the previous time point)

Ave average, SD standard deviation

* $p < 0.05$, Mann–Whitney test

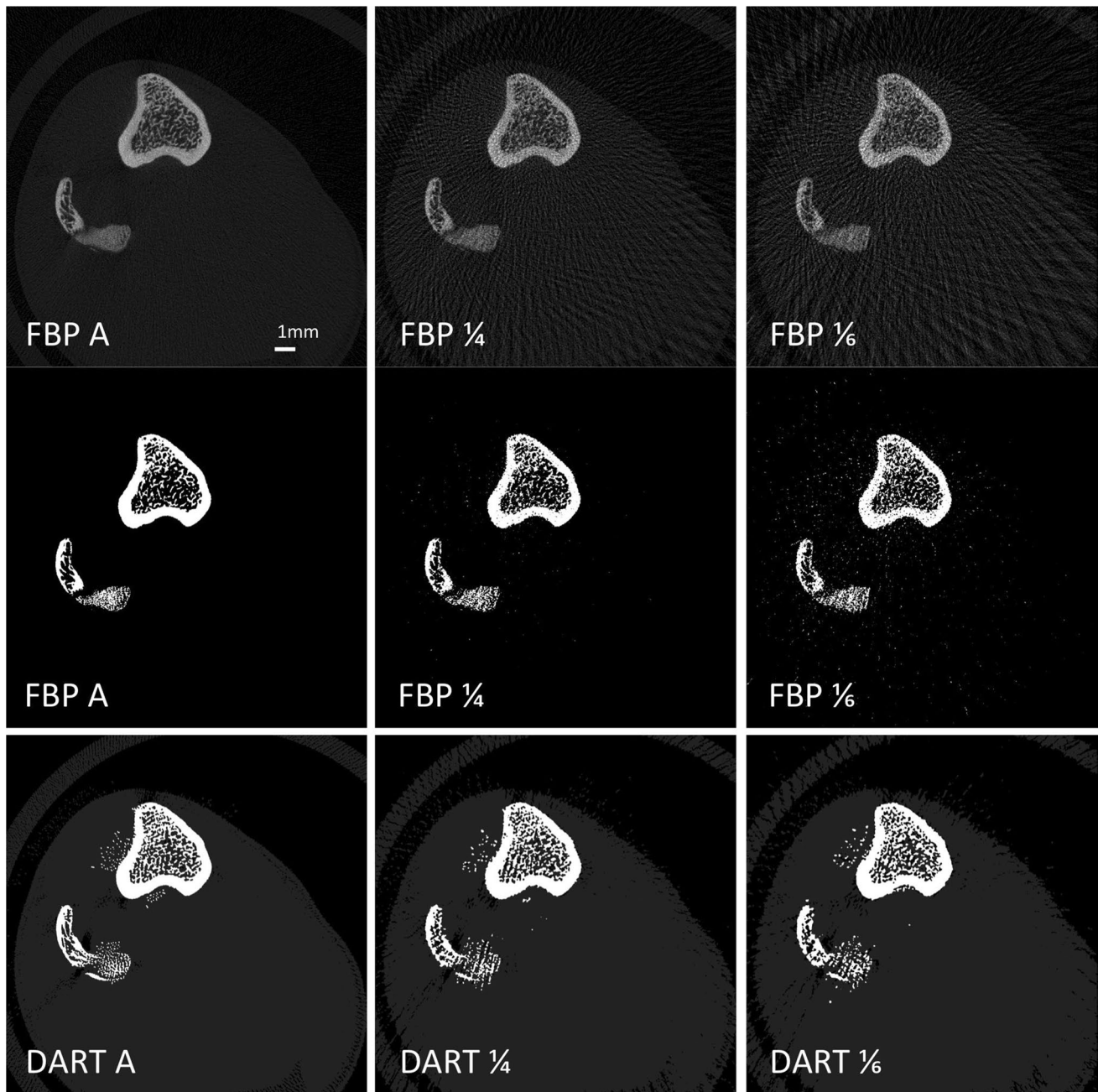


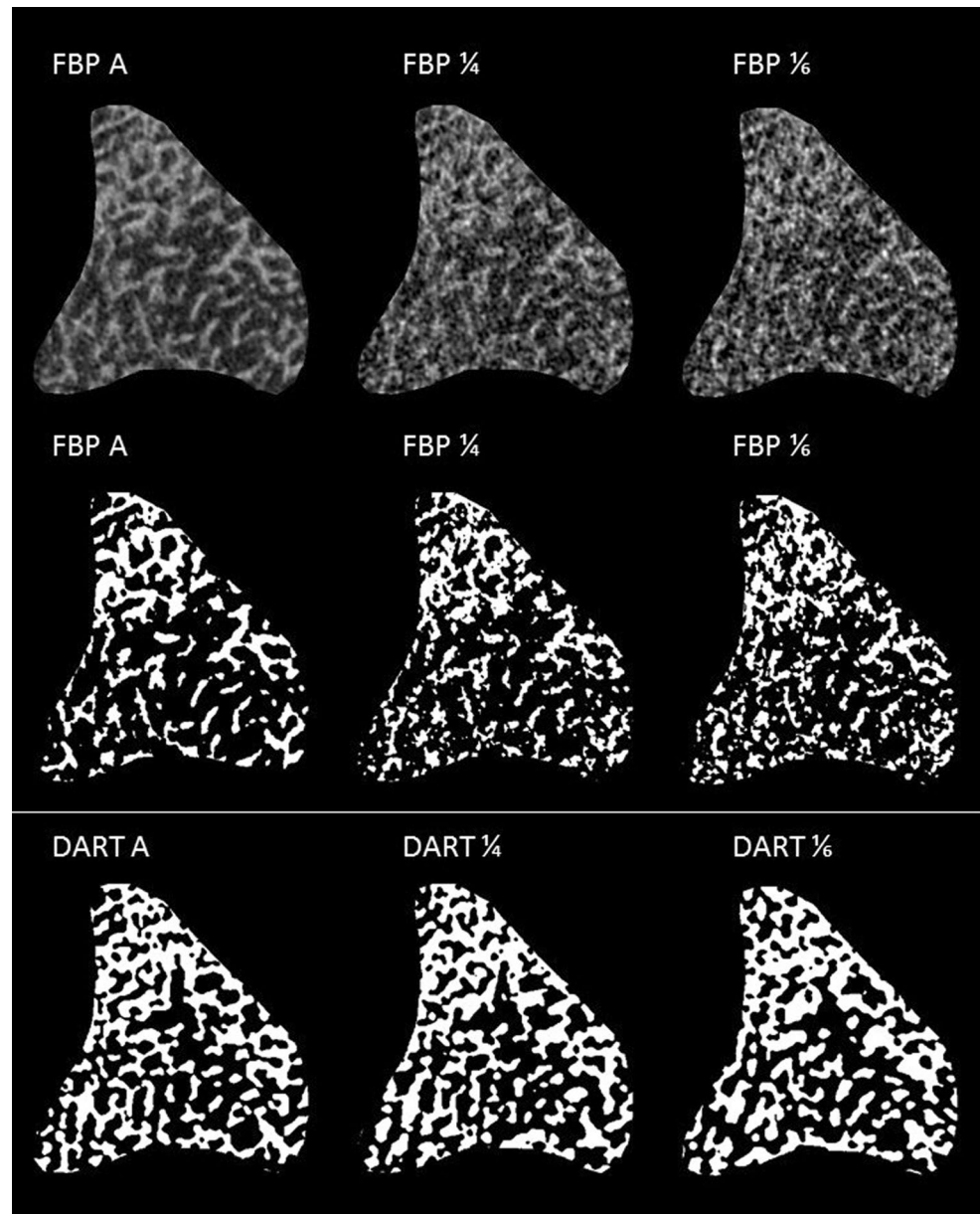
Fig. 1 Axial micro-CT cross-section image of a rat limb in a sham-operated rat at week 12. *Top row*: standard filtered back-projection reconstructions (grey level image) using all projections (FBP A), $\frac{1}{4}$ (FBP $\frac{1}{4}$) and $\frac{1}{6}$ (FBP $\frac{1}{6}$). *Middle row*: FBP after threshold-

ing, bone in white colour, background in black. *Bottom row* discrete tomography reconstructions with all projections (DART A), $\frac{1}{4}$ (DART $\frac{1}{4}$) and $\frac{1}{6}$ (DART $\frac{1}{6}$), where bone is white, background black and soft tissue grey

For DART, these projection-related differences were much smaller (3–5 or 5–7% in SHAM at $\frac{1}{4}$ or $\frac{1}{6}$, 0–5 or 0–8% in OVX, respectively) and not statistically significant at any time point. Similarly, other parameters, such as Tb.Sp and Tb.N, showed significant differences in the reduced compared to the full dataset; again, these were found mainly for FBP reconstructions (Table 4). For example, in OVX, when reducing the projections for the FBP, the Tb.Sp

progressively decreased by up to 68% of its original value (from 1078 to 685 μm or 348 μm , for all, $\frac{1}{4}$ or $\frac{1}{6}$ of the projections), approaching values close to the range of the SHAM group (231, 176 μm or 143 μm). Correspondingly, the Tb.N increased with fewer projections, with highest increases found particularly in the OVX group, up to +79% of its full-projection values. In DART, these differences were much lower and, in general, not statistically

Fig. 2 Same axial micro-CT cross-section image as in Fig. 1, but now showing only the trabecular bone region of interest used for analysis. *Top row*: standard filtered back-projection reconstructions (grey level image) using all projections (FBP A), $\frac{1}{4}$ (FBP $\frac{1}{4}$) and $\frac{1}{6}$ (FBP $\frac{1}{6}$). *Middle row*: FBP after thresholding and application of a noise despeckle filter (10 voxels), bone in white colour, background in black. *Bottom row*: discrete tomography reconstructions with all projections (DART A), $\frac{1}{4}$ (DART $\frac{1}{4}$) and $\frac{1}{6}$ (DART $\frac{1}{6}$), after application of a noise despeckle filter (10 voxels), bone in white colour, background in black



significant both for Tb.Sp (max 18% SHAM or 15% OVX, when reducing to $\frac{1}{6}$ of the projections) and Tb.N (max 14% SHAM, 16% OVX). Tb.Th showed significant increases over time for the SHAM and OVX group, for both methods. Reducing projection images to $\frac{1}{4}$ or $\frac{1}{6}$ significantly decreased Tb.Th for FBP (in SHAM up to -16% or -20% ; in OVX -15% or -25%), whereas it increased in DART (in SHAM, up to 14 or 24%; in OVX, 15 or 25%). SMI decreased over time in SHAM and increased in OVX, for both methods. With fewer projections, SMI increased for both methods and animal groups, reaching particularly high (and improbable) values for FBP $\frac{1}{6}$ OVX at weeks 8 and 12 (SMI = 3.2 and 3.4, respectively), compared to DART $\frac{1}{6}$ OVX (SMI = 2.5 and 2.6, respectively).

The Obj.N, when reducing the number of projection images, was significantly increased in the FBP reconstructions at all time points (up to a maximum of 1300% increase, $\frac{1}{6}$ FBP vs. all FBP projections, OVX week 12); this was not so in the DART reconstructions (Fig. 5). This increase in amount of objects is also visible in the reconstructed cross-section images (Figs. 1, 2) and in the 3D renderings (Fig. 3).

Discussion

When studying bone changes in an in vivo animal experiment it is important to keep the dose and scan time as

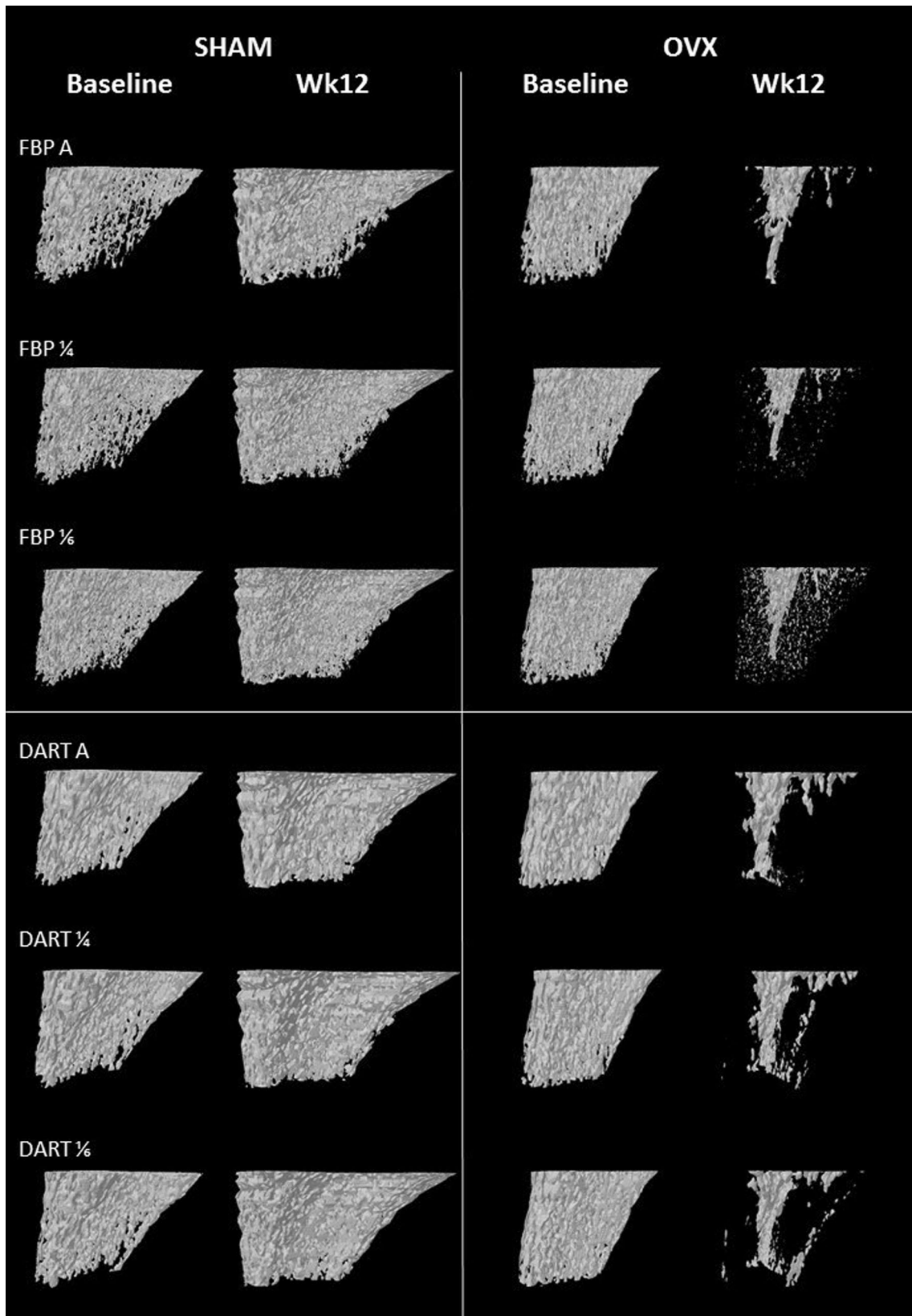


Fig. 3 3D micro-CT models of the trabecular bone VOI for a sham-operated and an OVX rat at baseline and week 12, using all projections (FBP A or DART A), $\frac{1}{4}$ (FBP $\frac{1}{4}$ or DART $\frac{1}{4}$) and $\frac{1}{6}$ (FBP $\frac{1}{6}$ or DART $\frac{1}{6}$)

low as possible without compromising the image quality and the morphological parameter calculations. One way of achieving this is by reducing the amount of projection images. However, by doing so, the data available for calculating an accurate reconstruction image using the standard FBP reconstruction techniques might not be sufficient. In this study, DART is presented as a valuable iterative reconstruction technique which is less sensitive to the decrease in projection images compared to FBP.

When comparing bone changes over time between the OVX and SHAM group by using FBP or DART reconstructions, the general trend observed in the morphometric parameters was independent of the reconstruction method. The two animal groups showed statistically significant between-group differences as well as time-related differences when compared to their own baseline (natural bone growth in SHAM, bone loss for OVX), although the actual values differed between the two reconstruction techniques (e.g., DART showed higher BV/TV values than FBP, for both rat groups).

Reduction of the number of projections had statistically significant effects, mainly for FBP. With a decreasing amount of projection images, there was an increase in noise speckles in the FBP reconstructions (Figs. 1, 2, 3), which led to an increase in Obj.N (Fig. 5). On the binary images, new random speckles appeared (noise) as well as some trabeculae became (artificially) broken. As a result, there were increases in BV/TV (between 6 and 58%, depending on the time point and animal group), statistically significant at 2 out of 5 time points (with more animals per group these would likely be significant at each time point). Other micro-architectural parameters, such as Tb.Sp, Tb.N and SMI, were significantly affected by the reduction of the projection images from the full dataset to 1/6 in FBP. The DART algorithm instead did not show this behavior, neither for BV/TV, nor for Tb.Sp, Tb.N and SMI, suggesting it to be more robust when reducing the number of projection images. Also the average Tb.Th decreased for FBP as a consequence of the appearance of small noise speckles in the images.

In the OVX group, a major amount of trabecular structure is lost by week 12. The increased noise due to reduced numbers of projections (Figs. 2, 3), particularly for FBP, apart from increasing BV/TV, drastically decreased the Tb.Sp, as the free space between adjacent trabeculae became smaller due to new speckles appearing, thus increasing also Tb.N and SMI (Fig. 4). SMI is a topological parameter, with values of 0, 3 and 4 indicating an ideal plate-like, rod-like and sphere-like structure, respectively [19]. An increase in SMI as seen for FBP, from SMI = 2.6 (merely a rod-like structure containing a few plates) to SMI = 3.4 when reducing all the projection images to 1/6, means that for the latter, there is the artificial presence of

sphere-like structures in the examined VOI, namely noise and disrupted trabeculae; indeed, an SMI value above 3 for trabecular bone is rather unrealistic. In contrast, for the DART algorithm, with a decrease in projection images, a substantially smaller spread in all the morphometric parameters is seen, with smaller and not significant differences compared to the full projection dataset. In fact, for DART in the OVX group, when reducing the full projection dataset to 1/6, the SMI increased from 2.0 to 2.1, a considerably smaller change compared to the FBP technique, maintaining also realistic values indicating a merely rod-like structure containing a few plates.

In this manuscript, DART was successfully applied to an *in vivo* micro-CT dataset of a rat model of osteoporosis and compared to FBP reconstructions, which is the standard method typically used in the micro-CT community. To the best of the authors' knowledge, this is the first time that DART has been applied to *in vivo* micro-CT scans. Our results suggest that DART can be a viable alternative method for quantitative morphometric studies. With reduced numbers of projections, DART performed at least as well and, in some instances, better than FBP, particularly when the projection numbers were considerably reduced (from full projections to 1/6, that is 248 to 42 images), with the morphometric parameters less affected by an increase in noise speckles. Future studies might investigate DART in animal models of different pathologies and with different acquisition conditions.

Whereas DART has shown great potential in the field of electron microscopy [11], its application in X-ray micro-CT so far has been limited to merely proof of concepts studies [12, 13]. Iterative algorithms pose a high computational burden, a reason why they might not have yet been widely used in X-ray micro-CT [8]. However, recent developments in high-performance computing have led to the acceleration of iterative techniques, such as using several GPUs [20]. In the present study, all reconstructions were performed on a computer containing an Intel Xeon E5-2630 CPU @2.30 GHz, 128 GB of memory and two NVIDIA Tesla K20Xm GPU's. We used the standard algorithm available at the Vision Lab, which usually handles smaller datasets and is not optimized for big datasets as these. Nonetheless, we attempted a comparison in computation time. A DART reconstruction (100 iterations) using all, 1/4 or 1/6 projection images required 51, 21 and 17 h to compute, respectively, which, compared to 7 min by using FBP with the GPU Reconsolver (1.6.6), might seem a rather long time. However, the DART algorithm can be significantly optimized by moving several parts of the algorithm to the GPU, which would drastically reduce the final reconstruction time. This is part of future work in our group.

The strength of discrete tomography is that a priori knowledge on the attenuation values of the sample is

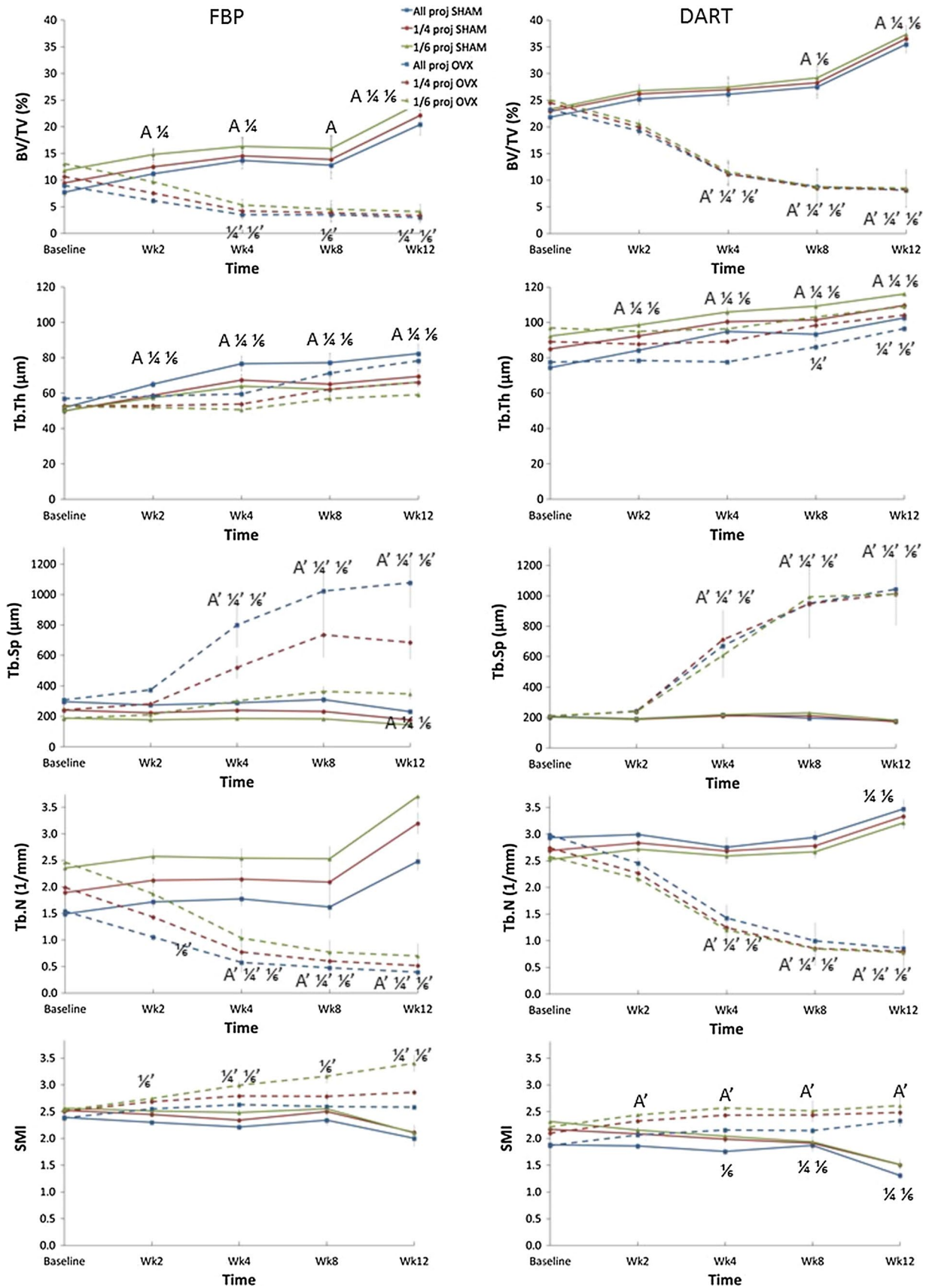


Fig. 4 Trabecular bone morphometric parameters (BV/TV, Tb.Th, Tb.Sp, Tb.N and SMI) monitored over time, for FBP (*left column*) and DART (*right column*) algorithm. A for SHAM, A' for OVX group: $p < 0.05$ compared to their baseline, for all projections (Mann–Whitney test). ¼ for SHAM, ¼' for OVX group: $p < 0.05$ compared to their baseline, for ¼ of the projections (Mann–Whitney test). 1/6 for SHAM, 1/6' for OVX group: $p < 0.05$ compared to their baseline, for 1/6 of the projections (Mann–Whitney test)

included in the reconstruction algorithm. The downside is that this prior knowledge has to be available, which, in practice, might not always be the case. DART has been reported to improve reconstructions over FBP in specimens containing a known amount of materials, or in challenging cases with non-equiaxial sampling, or when some projection data are missing, or with reduced number of projections [8]. Reducing the number of projection images reduces scanning time and related exposure to X-rays. If a typical scan lasts 20 min, a scan with 1/4 or 1/6 of the files requires 5 min or less than 4 min, respectively. The reduced radiation is an advantage ethically and experimentally, whereas the reduced scanning time is also an obvious practical advantage, particularly if many animals have to be scanned.

The limitation of this study is the low number of animals per group (three). For this reason, a non-parametric Friedman test was used instead of a parametric repeated measurement ANOVA statistical test. A Wilcoxon signed rank test (non-parametric analog to the paired t test) was not used for comparing time-related changes, or changes due to reduced projection images, as that statistical test would not give meaningful results for such small cohorts; a Mann–Whitney test was used instead.

DART relies on specific constraints of the grey levels in the reconstructed image, namely that the grey level intensity of each voxel corresponds to a specific class of attenuation values (and, hence, to a specific class of materials or tissues). However, in practice, physical effects present in X-ray micro-CT, such as noise, partial volume effect, beam hardening or scatter artefacts, which have an impact on the otherwise discrete grey levels, may call for less strict enforcement of these constraints in order to improve the accuracy of DART reconstructions. Future work might also consider the introduction of fuzzy classification into the DART algorithm in which classification parameters will be optimized by studying the residual reconstructed error [21]. Another further development of DART could be to account for the energy dependency of the (discrete) attenuation coefficients, which would enable a better assignment of each voxel to a specific attenuation class.

It could be questioned whether DART can be used for bone mineral density (BMD) analysis on a voxel scale (direct conversion of grey levels to BMD); since only a discrete amount of grey values are used when applying DART,

Table 3 OVX vs. SHAM groups, statistical significances in morphometric parameters at each time point (Mann–Whitney test)

Week	Baseline	Week 2	Week 4	Week 8	Week 12
BV/TV					
FBP ALL	ns	<0.05	<0.05	<0.05	<0.05
FBP ¼	ns	<0.05	<0.05	<0.05	<0.05
FBP 1/6	ns	<0.05	<0.05	<0.05	<0.05
DART ALL	ns	<0.05	<0.05	<0.05	<0.05
DART ¼	ns	<0.05	<0.05	<0.05	<0.05
DART 1/6	ns	<0.05	<0.05	<0.05	<0.05
Tb.Th					
FBP ALL	ns	<0.05	<0.05	ns	ns
FBP ¼	ns	<0.05	<0.05	ns	ns
FBP 1/6	ns	<0.05	<0.05	ns	ns
DART ALL	ns	<0.05	<0.05	ns	ns
DART ¼	ns	<0.05	<0.05	ns	ns
DART 1/6	ns	ns	<0.05	ns	<0.05
Tb.Sp					
FBP ALL	ns	<0.05	<0.05	<0.05	<0.05
FBP ¼	ns	<0.05	<0.05	<0.05	<0.05
FBP 1/6	ns	<0.05	<0.05	<0.05	<0.05
DART ALL	ns	<0.05	<0.05	<0.05	<0.05
DART ¼	ns	<0.05	<0.05	<0.05	<0.05
1/6 DART	ns	<0.05	<0.05	<0.05	<0.05
Tb.N					
FBP ALL	ns	<0.05	<0.05	<0.05	<0.05
FBP ¼	ns	<0.05	<0.05	<0.05	<0.05
FBP 1/6	ns	<0.05	<0.05	<0.05	<0.05
DART ALL	ns	<0.05	<0.05	<0.05	<0.05
DART ¼	ns	<0.05	<0.05	<0.05	<0.05
DART 1/6	ns	<0.05	<0.05	<0.05	<0.05
SMI					
FBP ALL	ns	<0.05	<0.05	ns	<0.05
FBP ¼	ns	<0.05	<0.05	ns	<0.05
FBP 1/6	ns	<0.05	<0.05	<0.05	<0.05
DART ALL	ns	<0.05	<0.05	ns	<0.05
DART ¼	ns	<0.05	<0.05	<0.05	<0.05
DART 1/6	ns	<0.05	<0.05	<0.05	<0.05

it is not possible to look at density differences on a voxel-by-voxel basis. However, it could be feasible to assess for mean density differences between different bone samples. The grey level values used in DART are estimated using a projection distance minimization method [17], which automatically finds the optimal threshold values of the different materials in a sample; if different bone samples have a different mean density, this can be detected by using this method.

In conclusion, DART and FBP, when applied in in vivo micro-CT scans of a rat model of osteoporosis, showed similar changes in morphometric parameters over time,

Table 4 Percent differences in bone morphometric parameters due to a decreasing number of projection images: 1/4 and 1/6 of the projection images vs. all projection images

Week	Baseline (%)	Week 2 (%)	Week 4 (%)	Week 8 (%)	Week 12 (%)
BV/TV					
FBP SHAM 1/4	23	12	6	9	8
FBP SHAM 1/6	53*	32	19	24	20
DART SHAM 1/4	5	4	3	3	3
DART SHAM 1/6	7	6	5	6	5
FBP OVX 1/4	19	23	20	10	12
FBP OVX 1/6	46	58*	52	30	37
DART OVX 1/4	5	3	0	-3	2
DART OVX 1/6	8	7	4	0	5
Tb.Th					
FBP SHAM 1/4	-4*	-10*	-12	-16	-16
FBP SHAM 1/6	-3*	-12*	-17*	-20	-19
DART SHAM 1/4	14*	10	6	9	7
DART SHAM 1/6	24*	17*	12*	17*	13*
FBP OVX 1/4	-7	-9*	-10	-13	-15*
FBP OVX 1/6	-8	-11*	-15*	-20*	-25*
DART OVX 1/4	15*	12*	15*	14*	8*
DART OVX 1/6	25*	21*	24*	20*	13*
Tb.Sp					
FBP SHAM 1/4	-19	-19*	-17	-25*	-24*
FBP SHAM 1/6	-37*	-36*	-36*	-41*	-38*
DART SHAM 1/4	-2	-2	-4	8	-3
DART SHAM 1/6	-2	0	0	18*	2
FBP OVX 1/4	-22	-25*	-35	-28	-36
FBP OVX 1/6	-40*	-44*	-62*	-65*	-68*
DART OVX 1/4	15	12	15	14	8
DART OVX 1/6	3	-2	-9	4	-3
Tb.N					
FBP SHAM 1/4	27	24	21	29	29*
FBP SHAM 1/6	58*	50*	43*	56*	49*
DART SHAM 1/4	-8	-5	-3	-6	-4
DART SHAM 1/6	-14	-9	-6	-9	-7
FBP OVX 1/4	29	36*	34	27	32
FBP OVX 1/6	60	78*	79	62	78
DART OVX 1/4	-8	-7	-13	-14	-6
DART OVX 1/6	-14	-12	-16	-15	-9
SMI					
FBP SHAM 1/4	6	6	6	7	6
FBP SHAM 1/6	7	9*	12*	9	5
DART SHAM 1/4	15*	12	13	2	15
DART SHAM 1/6	23*	16*	16	3	16
FBP OVX 1/4	5	5	6*	7	11*
FBP OVX 1/6	6	8	14*	22*	32*
DART OVX 1/4	12	12*	13*	14	7
DART OVX 1/6	18*	18*	19*	17	12

* $p < 0.05$ compared to all projection images; Mann–Whitney test

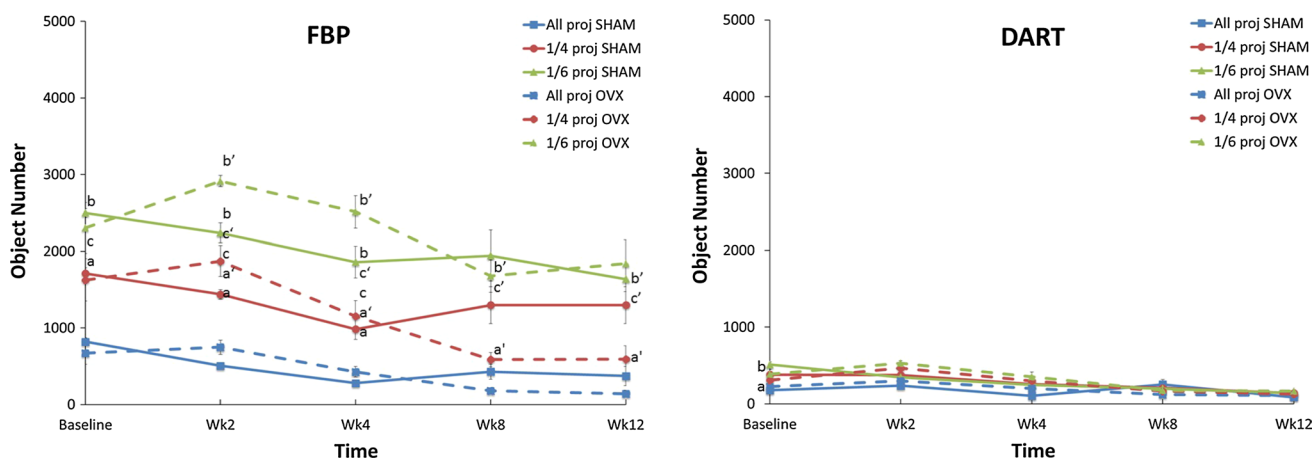


Fig. 5 The object number present in the 3D trabecular VOI calculated for the FBP (*left graph*) and DART (*right graph*), at different time points and number of projections. With decreasing number of projections (all, 1/4, 1/6), the object number is much more affected for FBP where it significantly increases up to over 1300% of its value (all projections vs. 1/6 for FBP, week 12, OVX), than for DART. *a* for SHAM, *a'* for OVX group; $p < 0.05$ between all projections and 1/4 of

the projections, for either FBP or DART (Mann–Whitney test). *b* for SHAM, *b'* for OVX group; $p < 0.05$ between all projections and 1/6 of the projections, for either FBP or DART (Mann–Whitney test). *c* for SHAM, *c'* for OVX group; $p < 0.05$ between 1/4 of the projections and 1/6 of the projections, for either FBP or DART (Mann–Whitney test). *s* statistical significances in morphometric parameters at each time point (Mann–Whitney test)

although the actual values were systematically overestimated (or underestimated) by DART. The DART algorithm was, however, more robust when using fewer projection images (62 or 42), where the standard FBP reconstruction was more prone to noise, showing a significantly bigger deviation from the morphometric parameters obtained using all projection images (248). This study supports the use of DART in X-ray micro-CT animal studies, in particular, when the number of projections has to be drastically minimized, which directly reduces scanning time and dose or when projections are missing.

Acknowledgements Funding for the experimental data used in this work was provided by a grant from the Australian Research Council (DP0663271). This work was supported by the Research Foundation–Flanders (FWO, Belgium) through project funding G0F9117 N and S004217 N, and by the University of Antwerp (TOP BOF project 26824).

Compliance with ethical standards

Conflict of interest The authors declare that there are no conflicts of interest to disclose.

References

- Perilli E, Le V, Ma B, Salmon P, Reynolds K, Fazzalari NL (2010) Detecting early bone changes using in vivo micro-CT in ovariectomized, zoledronic acid-treated, and sham-operated rats. *Osteoporos Int* 21:1371–1382
- Mohan G, Perilli E, Kuliwaba JS, Humphries JM, Parkinson IH, Fazzalari NL (2011) Application of in vivo micro-computed tomography in the temporal characterization of subchondral bone architecture in a rat model of low-dose monosodium iodoacetate-induced osteoarthritis. *Arthritis Res Ther* 13:R210. doi:10.1186/ar3543
- Perilli E, Cantley M, Marino V, Crotti T, Smith M, Haynes D, Dharmapatri A (2015) Quantifying not only bone loss, but also soft tissue swelling, in a murine inflammatory arthritis model using micro-computed tomography. *Scand J Immunol* 81:142–150
- Van Bael S, Chai YC, Truscello S, Moesen M, Kerckhofs G, Van Oosterwyck H, Kruth JP, Schrooten J (2012) The effect of pore geometry on the in vitro biological behavior of human periosteum-derived cells seeded on selective laser-melted Ti6Al4 V bone scaffolds. *Acta Biomater* 8:2824–2834. doi:10.1016/j.actbio.2012.04.001
- Wong HM, Yeung KWK, Lam KO, Tam V, Chu PK, Luk KDK, Cheung KMC (2010) A biodegradable polymer-based coating to control the performance of magnesium alloy orthopaedic implants. *Biomaterials* 31:2084–2096. doi:10.1016/j.biomaterials.2009.11.111
- Feldkamp L, Davis L, Kress J (1984) Practical cone-beam algorithm. *J Opt Soc Am A* 1:612–619
- Herman G (1980) Image reconstruction from projections: the fundamentals of computerized tomography. Academic press, New York
- Batenburg KJ, Sijbers J (2011) DART: a practical reconstruction algorithm for discrete tomography. *IEEE Trans Image Process* 20:2542–2553. doi:10.1109/TIP.2011.2131661
- Bals S, Batenburg KJ, Liang D, Lebedev O, Van Tendeloo G, Aerts A, Martens JA, Kirschhock CE (2009) Quantitative three-dimensional modeling of zeolite through discrete electron tomography. *J Am Chem Soc* 131:4769–4773. doi:10.1021/ja8089125
- Batenburg KJ, Bals S, Sijbers J, Kübel C, Midgley PA, Hernandez JC, Kaiser U, Encina ER, Coronado EA, Van Tendeloo G (2009) 3D imaging of nanomaterials by discrete tomography. *Ultramicroscopy* 109:730–740
- Batenburg KJ, Sijbers J, Poulsen HF, Knudsen E (2010) DART: a robust algorithm for fast reconstruction of three-dimensional grain maps. *Journal of Applied Crystallography* 43:1464–1473

12. van Aarle W, Van Gompel G, Batenburg KJ, Van de Castele E, Sijbers J (2010) A 3-dimensional discrete tomography approach for superresolution micro-CT images: application to foams. In: The first international conference on image formation in X-ray computed tomography 45–48
13. Van Gompel G, Batenburg KJ, Van de Castele E, van Aarle W, Sijbers J (2010) A discrete tomography approach for super-resolution micro-CT images: application to bone. In: IEEE International Symposium on Biomedical Imaging: From Nano to Macro, pp 816–819. doi:10.1109/ISBI.2010.5490111
14. Palenstijn WJ, Batenburg KJ, Sijbers J (2013) The ASTRA tomography toolbox. In: 13th International Conference on Computational and Mathematical Methods in Science and Engineering
15. van Aarle W, Palenstijn WJ, De Beenhouwer J, Altantzis T, Bals S, Batenburg KJ, Sijbers J (2015) The ASTRA Toolbox: a platform for advanced algorithm development in electron tomography. *Ultramicroscopy*. doi:10.1016/j.ultramic.2015.05.002
16. van Aarle W, Palenstijn WJ, Cant J, Janssens E, Bleichrodt F, Dabralovski A, De Beenhouwer J, Batenburg KJ, Sijbers J (2016) Fast and flexible X-ray tomography using the ASTRA toolbox. *Opt Express* 24:25129–25147
17. Batenburg KJ, Sijbers J (2009) Optimal threshold selection for tomogram segmentation by projection distance minimization. *IEEE Trans Med Imaging* 28:676–686
18. Zaiontz C (2015) Real statistics using Excel. <http://www.real-statistics.com>. Accessed 29 Dec 2016
19. Perilli E, Baruffaldi F, Bisi MC, Cristofolini L, Cappello A (2006) A physical phantom for the calibration of three-dimensional X-ray microtomography examination. *J Microsc* 222:124–134
20. Palenstijn WJ, Batenburg KJ, Sijbers J (2011) Performance improvements for iterative electron tomography reconstruction using graphics processing units (GPUs). *J Struct Biol* 176:250–253. doi:10.1016/j.jsb.2011.07.017
21. Roelandts T, Batenburg KJ, den Dekker AJ, Sijbers J (2014) The reconstructed residual error: a novel segmentation evaluation measure for reconstructed images in tomography. *Comput Vis Image Underst* 126:28–37